A Manipulability Criterion for Magnetic Actuation of Miniature Swimmers With Flexible Flagellum

Jérémy Begey, Maxime Etievant, Johan Quispe, Aude Bolopion, Marc Vedrines, Joël Abadie, Stéphane Regnier, Nicolas Andreff, Pierre Renaud

A Manipulability Criterion for Magnetic Actuation of Miniature Swimmers with Flexible Flagellum

J. Begey*,1,2,+, M. Etiévant*,2, J. Quispe*,3, A. Bolopion[2], M. Vedrines[1], J. Abadie[2], S. Régnier[3], N. Andreff[2], P. Renaud[1]

***Abstract*— The use of untethered miniature swimmers is a promising trend, especially in biomedical applications. These swimmers are often operated remotely using a magnetic field commonly generated using fixed coils that can suffer from a lack of compactness and heating issues. The analysis of the swimming capabilities is still an ongoing topic of research. In this paper, we focus on the ability of a magnetic actuation system to operate the propulsion of miniature swimmers with flexible flagellum. As a first contribution, we present a new manipulability criterion to assess the ability of a magnetic actuation system to operate a swimming robot, *i.e.* to ensure a displacement in any desired direction with a fixed minimum speed. This criterion is developed thanks to an analogy with cable-driven parallel robots. As a second contribution, this manipulability criterion is exploited to identify the dexterous swimming workspace which can be used to design of new coil configurations as well as to highlight the possibilities of moving coil systems. A case study for a planar workspace surrounded by three coils is in particular carried out. The accompanying video illustrates the application of the proposed criterion in 3D, for a large number of coils.**

I. Introduction

Positioning and steering magnetically actuated devices have attracted wide attention due to the large range of applications, in particular for the biomedical domain. Such a remote actuation approach was considered for minimally invasive operations, targeted drug delivery, displacement toward hard-to-reach areas, or micromanipulation [1, 2]. Magnetically actuated swimmers emerged as viable candidates for such tasks at a small scale in fluidic environments, but their control is still a challenge. By definition, in a low Reynolds number environment, viscous forces are indeed dominant. Thus, volumic forces tend to be negligible and the Navier-Stokes equation becomes time-independent [3, 4]. This is why it becomes fundamental to base swimming sequence on non-reciprocal animations [5], *i.e.* a succession of movements that do not counterbalance each other.

Magnetic actuation of micro-robots can be split into two categories, force-based, and torque-based approaches. The first one requires a magnetic gradient in order to induce pulling force [6, 7]. The second one is bio-inspired [8], using an analogy with the Escherichia Coli bacteria, rodhobacter spheroids, spermatozoon among others. The corkscrew-like motion and the undulating flexible flagella motion have been extensively reviewed in the literature [9, 10]. Alternatively, new locomotion methods have also been proposed using magnetic torques and forces. For instance, in [11], magnetic fields are used to obtain the displacement of a bio-inspired robot by deforming a soft multi-legged body. In [12], ferromagnetic ink is interestingly used during a 3D printing manufacturing process and allows to print soft materials with programmed ferromagnetic domains presenting new behaviors for locomotion.

In any case in liquid environment, as the size of the object decreases, the viscous forces become predominant compared to the volume forces. This phenomenon is discussed in [13] and it is then outlined that swimming with a magnetically driven helical or elastic-tail propulsion is more efficient compared to direct pulling on the body as the robot size decreases. Actuation through magnetic torques is then considered in this paper.

To operate the aforementioned robots, two main types of magnetic actuation systems have been developed. The first one is an arrangement of multiple stationary coils located around the workspace. Helmholtz (resp. Maxwell) coils are used to generate uniform field (resp. gradients) [7]. Magnetic-resonance-imaging devices are also used when strong gradients are required [14, 15, 16]. The magnetic field is then modulated thanks to current variations in the coil. These systems often suffer from low compactness, poor accessibility [17], and the need for active cooling when large currents are required [18]. In an alternative way, mobile permanent magnets have been also considered. Their relative displacements allow shaping the magnetic field obtained in the workspace [19, 20]. These kind of systems can produce fields of high intensity, well suited to control swimmers in a large workspace. Nevertheless, unlike electromagnet systems, the magnetic field produced by a permanent magnet device cannot be switched off, which can raise safety issues.

Considering the advantages and limitations of these two types of manipulation systems, a moving coil handling system was proposed in [21]. The concept was further developed with the DeltaMag system which comprises three electromagnets able to rotate about an axis [22], while the ARMM system employs a 6 Degrees-of-freedom mobile coil system [23]. Aiming to increase the size of the workspace while reducing coil heating issues, interest around moving coil architectures is growing. In this paper, we thus consider how to help to understand and design such systems.

*Authors equally contributed to the paper
+Corresponding author: jeremy.begey@etu.unistra.fr
1 ICube, Univ. of Strasbourg, INSA Strasbourg, Strasbourg, France
2 FEMTO-ST, Univ. Bourgogne Franche-Comté, CNRS, Besançon, France
3 ISIR, Sorbonne Univ., CNRS, Paris, France

Building magnetic navigation devices requires tools to characterize micro-robot behavior. When miniature swimmers are considered, kinematic analysis of the swimming abilities is then crucial. The evaluation of kinematic capabilities has been thoroughly studied in robotics by developing manipulability criteria. These criteria aim at determining the global capacity of a mechanism to generate velocities at a given pose of the workspace. The first manipulability criterion was proposed in [24] and variations have then been proposed, *e.g*. in [25]. To describe the capability to generate a velocity in any direction, *i.e*. to get an isotropic behaviour, other indices such as the conditioning index [26] have then been proposed. In [27], the authors develop such a criterion for a magnetic manipulation task based on the isotropy of the magnetic field or gradient. The evaluation was achieved through the study of an actuation system similar to the Octomag [7] . This criterion is then used to evaluate if isotropic kinematic performances can be obtained in an heterogeneous magnetic field.

In this paper and as the main contribution, we go beyond these results by proposing a complementary manipulability criterion to assess the ability of a magnetic actuation platform to propel a flexible swimmer in any direction at a minimum velocity. Such an index is of high interest to analyse the capabilities of a given system, to develop methods for the design of the magnetic actuation system and to propose new control laws. Through the closeness between the problem formulation of the wrench feasible workspace and the magnetic actuation formulation, the definition of this criterion and the way to derive it are proposed in analogy with kinematic assessment of cable-driven parallel robots. This criterion allows to analyze the swimming workspace of a flexible swimmer in a new way. The possibilities of new coil configurations and moving coil systems are then highlighted as a second contribution. In particular, a focus on the influence of moving coils on heating issues is proposed as it is a major limiting factor for implementation and safety of such devices.

A video showing the propulsion of the swimmer, the construction of the criterion and its computation on a case study is attached to the paper.
The paper is composed of five sections. We first raise the theoretical background for magnetic manipulation in Section II with a particular emphasis on the flexible swimmer manipulation. Section III focuses on the evaluation of the swimming performances and introduces the proposed manipulability criterion. Then Section IV depicts a case study. The propulsion requirements of a flexible swimmer are first experimentally determined in a controlled environment. The manipulability maps are then built using the proposed methodology. Simulation based on a reliable computation of the magnetic fields are presented to assess the results. Thanks to these maps, the advantages of the use of mobile coils are highlighted. Conclusions and perspectives are drawn in Section V.

II. Magnetic propulsion foundations

A. Magnetic actuation

In a general case, magnetic forces and torques are applied to move a micro-robot. To do so, we consider a magnetic actuation system composed of a set of coils located around the workspace in which a miniature magnetic swimmer is placed.
When a magnetic element, described by its dipole moment $\mathbf{m}$, is immersed in a quasi-static magnetic field $\mathbf{b}$, it experiences a magnetic force $\mathbf{f}$ and a torque $\mathbf{t}$ given by:

$$\mathbf{f} = \nabla(\mathbf{m}\cdot\mathbf{b}) = (\mathbf{m}\cdot\nabla)\,\mathbf{b} \tag{1}$$

$$\mathbf{t} = \mathbf{m}\wedge\mathbf{b} \tag{2}$$

In the following, we consider that the magnetic superposition theorem holds. This is well verified when using coreless coils, for which magnetic coupling can be neglected. When soft-magnetic core electromagnets are used, this assumption is valid as well, under the hypothesis detailed in [7]. The magnetic field amplitude is then varies linearly with respect to the current in the coil. Thus, the magnetic field at a given point $\mathbf{p}$ can be computed as the sum of the magnetic fields generated by each coil:

$$\mathbf{b}(\mathbf{p}) = \sum_{j=1}^{n} \mathbf{b_j}(\mathbf{p}) = \sum_{j=1}^{n} i_j \tilde{\mathbf{b_j}}(\mathbf{p}) \tag{3}$$

with n the number of coils, $\mathbf{b_j}$ the field contribution of the coil j, $\tilde{\mathbf{b_j}}$ the unit-current contribution, and i_j the electric current of the coil j with $j = \{1,\dots,n\}$. Because of hardware limitations, the coil current is $i_j \in [-i_{max}, i_{max}]$. Equation (3) can be reformulated as:

$$\mathbf{b}(\mathbf{p}) = \begin{bmatrix}\tilde{\mathbf{b_1}}(\mathbf{p}) & \dots & \tilde{\mathbf{b_n}}(\mathbf{p})\end{bmatrix} \begin{bmatrix} i_1 \\ \vdots \\ i_n \end{bmatrix} = \mathcal{B}(\mathbf{p})\mathbf{i} \tag{4}$$

with $\mathcal{B}(\mathbf{p})$ the $m \times n$ matrix mapping the currents to the magnetic field [7, 27] with m the dimension of the swimming space, *i.e*. $m = 2$ in the plane and $m = 3$ in the space. The *j-th* column of $\mathcal{B}(\mathbf{p})$ is the magnetic field produced along the cartesian coordinates by the *j-th* coil at the considered point $\mathbf{p}$.

B. Swimming propulsion

When moving in a fluid media, the Reynolds number reflects how the robot should act. In a low Reynolds number environment, the volumic forces exerted on it tend to be negligible compared to the viscous ones. Thus, it becomes energetically unattractive to exert a magnetic force to move the robot. This is why swimmers are used. Only the magnetic field $\mathbf{b}$ drives them [13].
To compute the velocity of the swimmer based on the efforts applied on it, a propulsion matrix has been introduced for helical swimmers in [3], then developed in [13]. This is no such simple relationship for a flexible swimmer. That is why experimental evaluations are performed in this paper to determine the velocity of the swimmer actuated by a

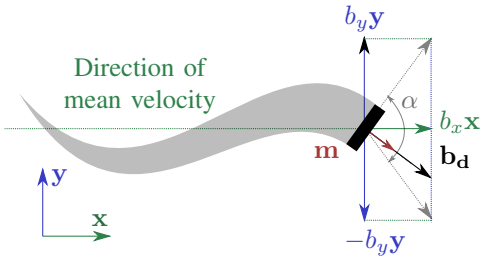

Fig. 1: Notations used for the propulsion foundations of a miniature swimmer with flexible flagellum.

magnetic field.

Miniature swimmers have to perform non-reciprocal patterns to self-propel [3]. An additional requirement is related to the ratio between viscous forces and elastic forces, described by a scalar value designated as the sperm number [28]. This number describes how flexible or rigid the robot structure should be for an efficient swimming. To achieve a good robot performance, the sperm number should be in the order of 1 [13, 29]. This constraint can be tuned for a given environment by adapting the robot geometry or material as well as using a suitable oscillation frequency.

Regarding the actuation magnetic field, this latter can be decomposed into driving and steering magnetic fields (respectively $\mathbf{b_d}$ and $\mathbf{b_s}$) as follows:

$$\mathbf{b} = \mathbf{b_d} + \mathbf{b_s} \tag{5}$$

Without loss of generality, we can consider that the robot moves in a direction denoted $\mathbf{x}$. To induce this displacement, an oscillating field has then to be created around this swimming direction. Let $\mathbf{y}$ be an orthogonal direction to $\mathbf{x}$. In [28], the expression of the driving magnetic field $\mathbf{b_d}$ is given by:

$$\mathbf{b_d} = b_x\,\mathbf{x} + b_y\cos(\omega t)\mathbf{y} \tag{6}$$

with b_y the oscillation amplitude, and b_x the magnitude of magnetic guidance as displayed in Fig. 1.

Swimming motion requires a minimal magnetic torque. This torque is linked to the values of b_x and b_y for a given oscillation frequency (Eq. (2)). Thus, a minimal magnetic field is needed to achieve the desired swimming motion.

III. Analysis of the Swimming Performances

A. Analysis of the magnetic field

So that a swimmer located at a position $\mathbf{p}$ moves at a desired minimal velocity v_{min}, a minimal magnetic field magnitude must be ensured. It is denoted b_{min} in the following. The magnetic field amplitude b_e along a direction $\mathbf{e}$ is given for the configuration vector $\mathbf{q}$ which reflects the poses of the coils at a given position $\mathbf{p}$ by:

$$b_e(\mathbf{q},\mathbf{p}) = |\sum_{j=1}^{n} \mathbf{b_j}(\mathbf{q},\mathbf{p})\cdot\mathbf{e}| \tag{7}$$

To obtain swimming capabilities, the condition (8) below must be ensured for given $\mathbf{q}$ and $\mathbf{p}$.

$$b_e(\mathbf{q},\mathbf{p}) \geq b_{min} \tag{8}$$

The respect of such a condition is indeed analog to a well-known problem for Cable-Driven Parallel Robots (CDPR) with the determination of the Wrench-Feasible Workspace (WFW). Cable-driven parallel robots are composed of a platform attached to the base frame with actuated cables which are in tension. To ensure that the cables are always pulling and prevent their deterioration, their tensions are usually bounded [30]. The WFW is the reachable workspace for a set of wrenches that can be applied to the platform while the tensions of the cables stay in their limits. To determine this WFW, a zonotope of reachable wrenches can be built for a simple end-effector pose using the tension limits in the cables [31]. As defined in [32], a zonotope is a vector sum of a finite number of closed line segments in some Euclidean space. The zonotope zone(Y) is expressed as in [31], with $\mathrm{Y} = \{\mathbf{y}_1, \mathbf{y}_2, \dots \mathbf{y}_n\} \in \mathbb{R}^d$ a set of vectors:

$$\mathrm{zone(Y)} = \left\{ \mathbf{x} \in \mathbb{R}^d | \mathbf{x} = \sum_{j=1}^{n} \alpha_j \mathbf{y}_j,\ 0 \leq \alpha_j \leq 1 \right\} \tag{9}$$

For a CDPR a wrench is part of the WFW if it is included in a zonotope-shaped set called available wrench set defined for a given pose of the platform.

In our context, the available magnetic fields that can be generated by n coils in the space are included in the set $\mathrm{A_B}$ defined using Eq. (3):

$$\mathrm{A_B} = \left\{ \mathbf{b}(\mathbf{p}) \in \mathbb{R}^m | \mathbf{b}(\mathbf{p}) = \sum_{j=1}^{n} i_j \tilde{\mathbf{b_j}}(\mathbf{p}),\ |i| \leq i_{max} \right\} \tag{10}$$

with m the dimension of the swimming space. It is interesting to note that the set $\mathrm{A_B}$ can then be expressed as a zonotope, with $\mathrm{B} = \{\tilde{\mathbf{b_1}}, \tilde{\mathbf{b_2}}, \dots \tilde{\mathbf{b_n}}\} \in \mathbb{R}^m$:

$$\mathrm{A_B} = \mathrm{zone}(\{i_{max}\mathrm{B}, -i_{max}\mathrm{B}\}) \tag{11}$$

An analogy with the determination of the WFW can then be carried out to characterize the swimmer propulsion.

B. Magnetic swimming manipulability

Here, we propose a new manipulability criterion for miniature swimmers noted $\mu(\mathbf{q},\mathbf{p})$ which represents the ability to propel in any direction at a minimum velocity for given $\mathbf{q}$ and $\mathbf{p}$. $\mu(\mathbf{q},\mathbf{p})$ is defined as the maximal magnetic field that can be generated along all directions (see attached video). This criterion is then analogous to the search of the maximal wrench that can be applied along all directions to a CDPR such as it stays in the WFW. Therefore, it is the radius of the largest sphere of center $\mathbf{p}$ for a given $\mathbf{q}$ that is inscribed in $\mathrm{A_B}$. This sphere is also called a Chebyshev ball, which is the general term for the largest Euclidean ball inscribed in a polytope [33]. In our case, the radius of this ball can be expressed as:

$$\mu(\mathbf{q},\mathbf{p}) = \min_{\mathbf{e}} |\sum_{j=1}^{n} \mathbf{b_j}(\mathbf{q},\mathbf{p})\cdot\mathbf{e}| \tag{12}$$

A Chebychev ball, and so the manipulability $\mu(\mathbf{q}, \mathbf{p})$, can be determined in several ways [33]. We here exploit the fact that $\mu(\mathbf{q}, \mathbf{p})$ is the minimal distance between the position $\mathbf{p}$ and the limits of $\mathrm{A}_{\mathcal{B}}$. The faces of a zonotope are supported by hyperplanes [31]. The distance d between the point P defined by the position $\mathbf{p}$ and one hyperplane is expressed as:

$$d = \frac{\mathbf{n} \cdot \mathbf{hp}}{\|\mathbf{n}\|} \tag{13}$$

with H a point of the hyperplane and $\mathbf{n}$ a normal vector to the hyperplane. To compute the manipulability, the distance between P and each hyperplane supporting $\mathrm{A}_{\mathcal{B}}$ is determined using Eq. (13). Finally, the smallest distance is identified and it is the manipulability $\mu(\mathbf{q}, \mathbf{p})$.

C. Dexterous swimming space

The manipulability criterion $\mu(\mathbf{q}, \mathbf{p})$ is then used to define the dexterous swimming space $\mathrm{W_s}$. This swimming space is the set of swimmer positions in which no limitation on the swimming directions exists, to ensure the desired performance v_{min} for a configuration $\mathbf{q}$. The latter is defined as the set of coil poses included in all eligible configurations Q. For sake of clarity of the notations, the dependency in $\mathbf{q}$ and $\mathbf{p}$ is omitted. The dexterous swimming space is then expressed as:

$$\mathrm{W_s} = \{\mathbf{p} \mid \exists\, \mathbf{q} \in \mathrm{Q} \text{ where } \mu \geq b_{min}\} \tag{14}$$

To illustrate these notions, a simplified example with two coils in the plane is provided in Fig. 2. For such a case, $\mathrm{A}_{\mathcal{B}}$ is a parallelogram. The Chebyshev ball inscribed in this parallelogram is a circle, represented in green dashed line, and which defines the manipulability μ. From Fig. 2, we can directly observe if the position $\mathbf{p}$ is in the dexterous swimming space $\mathrm{W_s}$ by comparing the radius μ with b_{min}. We can see that in configuration #1 (Fig. 2a) b_{min} is included in the set of magnetic fields that can be generated, *i.e.* $b_{min} < \mu$. Then, $\mathbf{p} \in \mathrm{W_s}$. However, in configuration #2 (Fig. 2b) b_{min} can not be reached in most of the directions as $b_{min} > \mu$. Therefore, if the coils are fixed and $\mathrm{Q} = \mathbf{q}$, $\mathbf{p} \notin \mathrm{W_s}$.

Based on an analogy with analysis methods used for cable-driven parallel robots, the manipulability index for miniature swimmers as well as the dexterous swimming space were proposed. The mathematical foundations of the proposed tools are generic in coil number and space dimension. This criterion can then be used to analyze actuation systems composed of any finite number of coils, in 2D or 3D space and considering any available coil configurations. As an illustration, the zonotope and the manipulability are computed for an Octomag-like system, *i.e.* in 3D space and with 8 coils, and the results are displayed in the attached video.

IV. Case Study

In the following, a case study is presented to illustrate the methodology proposed in the previous section. This study is composed of two parts. First, the requirements in terms of minimal magnetic field $\mathbf{b_{min}}$ necessary to propel the swimmer at a minimum velocity v_{min} is determined experimentally in a controlled environment. Second, the magnetic field in the whole swimming space is computed using a numerical method proposed in [34] and the manipulability maps are computed.

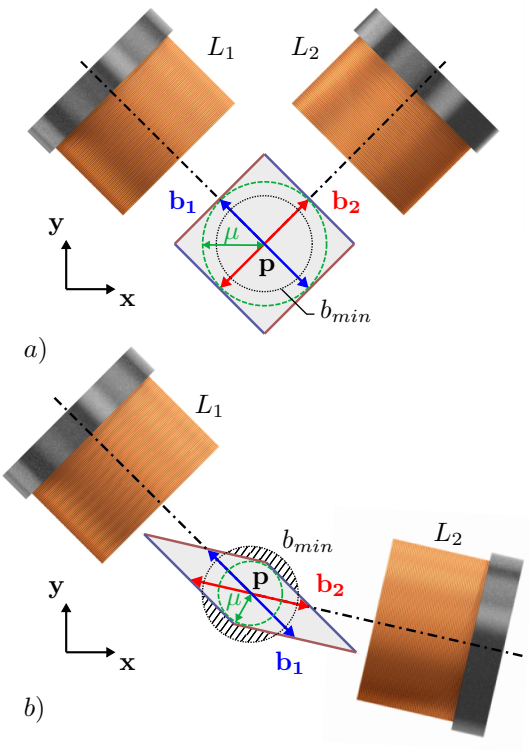

Fig. 2: Schematic representation of the magnetic field that can be generated thanks to two identical coils. Coils L_1 and L_2 are represented with dashed axes, the arrows describe the magnetic field of each coil at point $\mathbf{p}$ for $\pm i_{max}$ and the gray area represents $\mathrm{A}_{\mathcal{B}}$. The dotted circle represents the magnetic field required b_{min} to obtain the desired propulsion. The dashed green circle is the limits of the Chebyshev ball inscribed in $\mathrm{A}_{\mathcal{B}}$ which is used to compute the manipulability. The hatched areas depict the needed magnetic fields that cannot be generated. a) Configuration #1 coil axes are orthogonal. b) Configuration #2 coil axes are almost co-linear.

A. Assessment conditions

For sake of clarity, the case study is carried out with planar motions in the xy plane. The target swimming space is disc-shaped with a 150 mm diameter.

An actuation system composed of three coreless coils is considered. The coils must not penetrate the swimming space. The minimal distance r_0 between the center of the swimming space and the coil edge is then set. The coils can be displaced by rotation around the swimming space center with a radius r_0, keeping the coil axes intersecting at this center. In this way, the distance between coils and the swimming center is always minimum, which maximizes the intensity of the magnetic field. The coil configurations are defined by the angles θ_k, $k = \{1, 2, 3\}$ as illustrated in Fig. 3. The swimmer position is denoted $\mathbf{p}$ and the coil

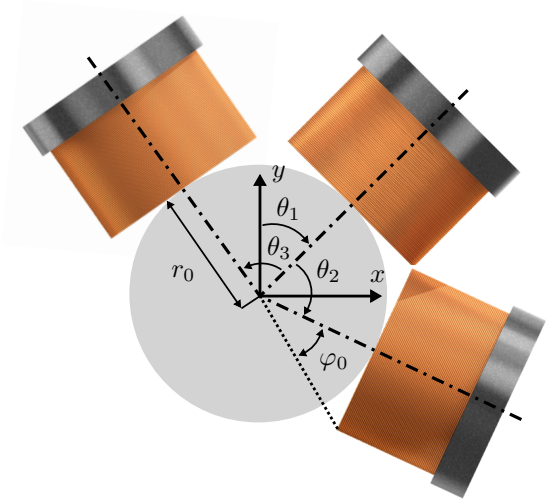

Fig. 3: Considered system to illustrate the methodology proposed to evaluate the dexterous swimming space. It is composed of three coils in the *xy* plane with their axis in dashed lines and the swimming space in light gray.

configuration $\mathbf{q}$ with

$$\mathbf{q} = [\theta_1, \theta_2, \theta_3]^T \tag{15}$$

B. Swimmer description and minimal magnetic field determination

To determine experimentally the magnetic field that must be produced to generate a minimum velocity v_{min}, a centimetric swimmer presented in Fig. 4a) is considered. The swimmer's tail is fabricated using a silicone elastomer. The tail is glued to a 1-mm disc-shaped Neodymium magnet. To emulate the behaviour of the robot at a small scale, pure glycerol is used to produce a low Reynolds number environment, as in [35]. In our case, the Reynolds number has an order of magnitude about 10^{-5}. Experiments are carried out by measuring the forward speed of the swimmer for different magnetic field amplitudes using a 3D Helmholtz coil system. This setup allows to generate a uniform magnetic field avoiding magnetic force disturbances. The system was calibrated by measuring the magnetic field at the center of the workspace by a Hirst GM08 magnetometer. The measurements are performed for b_x and b_y (see Eq. (6)) in $[0, 2]$ mT with a step of 0.5 mT. For this field magnitude, the cut-out frequency being about 1.5Hz, experiments were conducted with an oscillation frequency of 1Hz. For all experiments, the robot is 3D tracked through a visual servoing technique based on ViSP libraries. Each experiment is carried out for more than 80 seconds to estimate the average robot speed.

With $b_y = 0$ mT, the robot should stay stationary since there is no oscillatory part. However, when velocities are computed, a drift generated by different factors, *e.g.* tracking error, or parasitic magnetic field gradients, is observed. It has a value of 0.003 mm/s. This can be considered as noise on the velocity measurements.

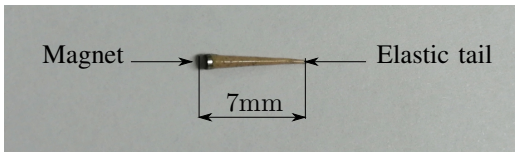

a) Flexible robot geometry

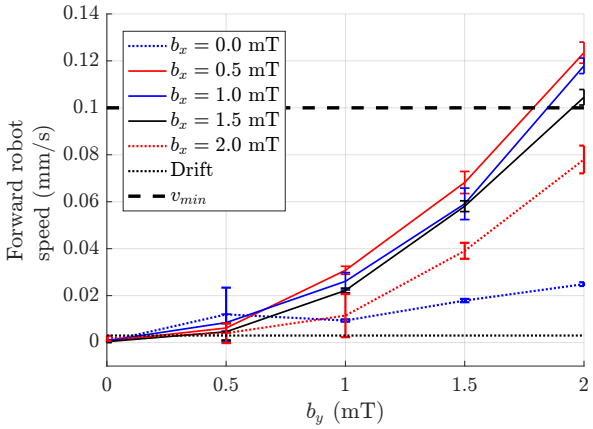

b) Robot response for different magnetic fields

Fig. 4: Flexible robot description and experimental evaluation of its swimming velocity. a) Flexible robot dimensions. b) Experimental forward speed of the swimmer for different magnetic amplitudes at 1 Hz.

In Fig. 4b) the robot speed is depicted for the aforementioned range of magnetic field components b_x and b_y. According to the results, an increase of the oscillation component b_y tends to increase the forward speed. Similarly, the decrease in the steering component b_x results in some improvement in speed up to some extent. This behaviour can be explained through the robot oscillation angle α. This angle is defined as $\alpha = 2\arctan(b_y/b_x)$ and is represented in Fig. 1. When the oscillation angle increases, the robot bends much more properly up to a certain point. Thus, it generates a larger thrust and forward speed is increased. Nevertheless, when the component b_x is nearly null, the oscillation angle tends toward $\pi/2$ and does not generate a proper tail bending.

The selection of v_{min} should be based on the application requirements. Here, the minimal swimming velocity is then arbitrarily set to $v_{min} = 0.1$ mm/s. This value does not impact the nature of the discussion conducted in the rest of the paper. Using the results displayed in Fig. 4b) multiple choices of b_x and b_y are available. We choose the one with the lowest norm among the measured points. Therefore, it leads to $b_x = 0.5$ mT and $b_y = 2$ mT. Finally, it yields to $b_{min} = 2.06$ mT.

C. Dexterous swimming space with fixed coils

To evaluate the dexterous swimming space that can be expected with such a system, numerical analyses are carried out to compute manipulability maps. First, we consider fixed coils. Two typical coil configurations are chosen. First, an intuitive configuration with the coils uniformly distributed

around the swimming space is selected, *i.e.* $\theta_1 = 0$ rad, $\theta_2 = -2\pi/3$ rad and $\theta_3 = 2\pi/3$ rad (Fig. 5a). Second, the configuration which maximizes the minimal value of the manipulability in the whole swimming space is chosen. This configuration cannot be trivially determined. Its determination was achieved by first computing manipulability maps with the proposed criterion for all possible coil configurations, *i.e.* all the possible coil poses without collisions. It was then observed that the best configuration corresponds to the case where the coils are gathered at the top of the swimming space with $\theta_1 = 0$, $\theta_2 = -2\varphi_0$ and $\theta_3 = 2\varphi_0$ (Fig. 5b). The angle φ_0 is defined in Fig. 3 and is expressed as:

$$\varphi_0 = \arctan\left(\frac{r_{coil}}{r_0}\right) \tag{16}$$

To compute and display the dexterous workspace maps, the swimming space is discretized with a grid of 60×60 points and the manipulability μ is computed for each one of them for a given current limit. The coils are composed of 40×110 loops and have a radius $r_{coils} = 50$ mm. To compute the field generated by a single coil $\mathbf{b_j}$, we used the elliptical integral formulation proposed in [34]. We then use $i_{max} = 1$ A to generate unitary maps which correspond to the unit current contribution proposed in Eq. (3). These results can easily be extrapolated to other values of i_{max} by scaling the maps with a factor of i_{max}. The maps obtained for the first and second coil configurations are displayed in Fig. 5a) and in Fig. 5b).

When uniformly distributed coils are considered, only a small dexterous workspace is obtained in the center of the swimming space for $i_{max} = 1$ A. Moreover, four distinct areas separated by a low manipulability region can be observed. In the low manipulability area, there exist configurations where μ can be close to 0 with a minimal value of 0.37 mT. It means that there is at least one direction along which the required magnetic field cannot be generated, *i.e.* $\mathcal{B}$ is rank deficient. In analogy with the kinematic analysis of conventional robots discussed in Section III, we can consider these configurations as close to singularities. The magnetic field being proportional to the current and as $b_{min} = 2.06$ mT, it means that a current of 5.56 A is required to ensure that the whole swimming space is dexterous, *i.e.* $\mu \geq b_{min}$.
Actions of avoiding or going through such singular configurations have been thoroughly studied in serial and parallel robotics. It might then be possible to find ways to reach the whole swimming space with the miniature swimmers. However, it would certainly require specific control schemes and trajectory planning that can be avoided by proper selection of coil configuration as outlined below.

In the second configuration, when the coils are gathered on top of the swimming space, no singularity is observed. However, as the magnetic field decreases with the distance, the bottom side of the swimming space presents low manipulability values. For $i_{max} = 1$ A, the lowest manipulability value is of 0.55 mT. In this case, a current of 3.74 A is needed to obtain a fully dexterous swimming space.

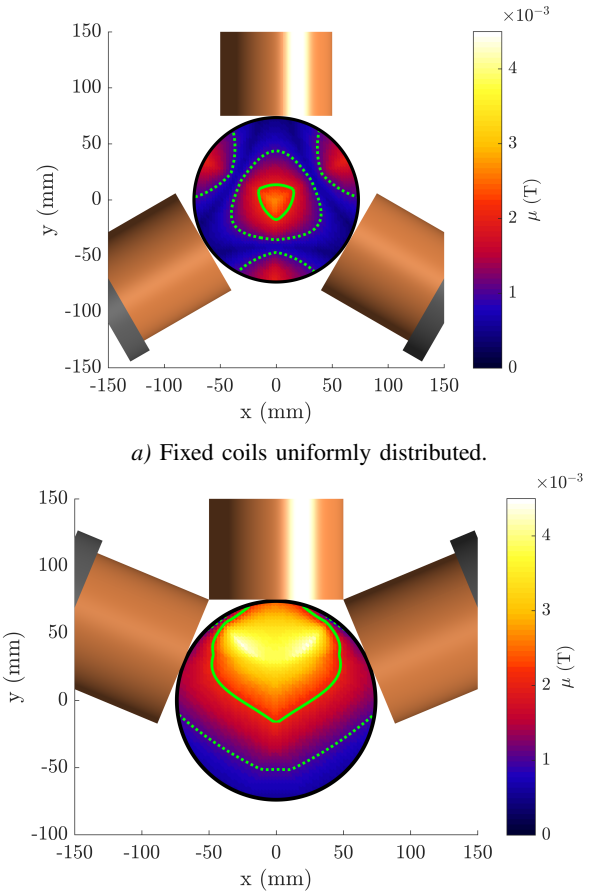

a) Fixed coils uniformly distributed.

b) Fixed coils gathered.

Fig. 5: Manipulability maps displayed in the *xy* plane for $i = 1$ A. Colors represent the manipulability. In green, the level lines for $b_e = b_{min} = 2.06$ mT and $b_e = 1$ mT, in plain and dotted lines respectively. a) Fixed coils uniformly distributed around the swimming space. b) Fixed coils gathered at the top side of the swimming space.

D. Dexterous swimming space with moving coils

We now consider that the pose of the coils can be dynamically modified. The angular ranges of the coils are chosen to avoid collisions and are expressed as:

$$\begin{cases} -\frac{\pi}{2} & \leq \theta_1 \leq \quad \frac{\pi}{2} \\ \varphi_0 - \pi & \leq \theta_2 \leq \quad -2\varphi_0 \\ 2\varphi_0 & \leq \theta_3 \leq \quad \pi - \varphi_0 \end{cases} \tag{17}$$

A manipulability map could be displayed for each eligible configuration of the coils. However, to better visualize the dexterous swimming spaces we can obtain, the maximum manipulability for all available $\mathbf{q} \in \mathrm{Q}$, with Q defined by the system of equations (17), is displayed in Fig. 6. With the use of coil reconfigurations, the minimum manipulability in the whole swimming space is equal to 2.0 mT. It means that to obtain a minimal manipulability of 2.06 mT, the current limit needs to be set to 1.03 A.

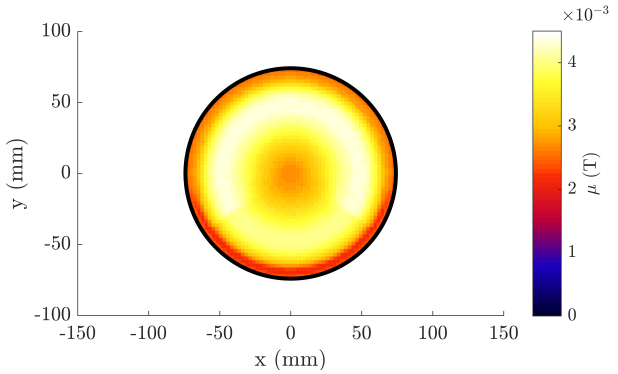

Fig. 6: Maximum manipulability obtained at each point for all possible poses of the coils and for $i = 1$ A.

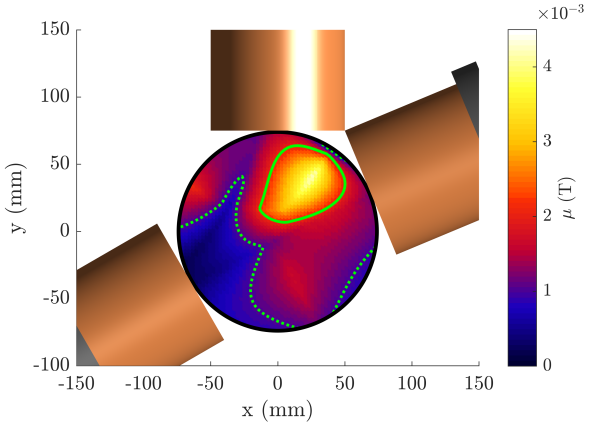

Fig. 7: Manipulability map obtained for $\theta_1 = 0$ rad, $\theta_2 = -2\varphi_0$ rad and $\theta_3 = 2\pi/3$ rad for $i = 1$ A.

In Fig. 7, $\mathbf{q}$ is chosen to obtain a compromise between the two fixed coil configurations proposed previously. The manipulability map of such configuration is interesting as it shows that the positions of the singularities observed in Fig. 5a) are modified. Thanks to moving coils, it is also possible to change the singular configurations.

These results are presented to illustrate the methodology proposed in III. For sake of clarity, a magnetic actuation system composed of 3 coils, and planar displacements are presented in this case study. However, the methodology is generic and can be applied in 3D to complex actuation system, as demonstrated in the accompanying video.

E. Discussion

Adding motions to the coils is interesting in several ways, whether the whole set of coils is moved or only relative motions between the coils are carried out. First, it allows modifying the shape of the manipulability maps to be able to reach the whole swimming space. In particular, when the relative poses of the coils are modified, the manipulability maps change allowing to move the singularities whereas simultaneous motions of the whole set of coils tend to improve the overall manipulability. Second, with this example, the needed current to ensure dexterity in the whole swimming space has been reduced from 5.56 A and 3.74 A to 1.03 A, *i.e.* by a factor of 5.4 and 3.6, thanks to simple coil motion identified by the use of the proposed manipulability criterion. The joule effect being a function of the square of the current, it means that the power leading to the coil heating is diminished by a factor of 29 and 13. The system is then less affected by coil heating issues, thus lowering the overall price as well as the design complexity of cooling systems. Moreover, it allows reducing the temperature of the environment which can be of interest, *e.g.* when considering bio-medical applications or when manipulating cells.

Moving coils may also be interesting as it allows to adjust local behavior and even singularity locations. The latter may be exploited to restrict the swimming space when obstacles must be avoided or if a restricted swimming space is desired for safety reasons. In particular, it can be seen from Fig. 7 that it is possible to have multiple high manipulability areas separated by low manipulability ones or singularities. This means exploiting mobile coils could help for independent control of multiple swimmers.

V. Conclusions and Perspectives

In this paper, we proposed a manipulability criterion to assess the capacity of a magnetic actuation platform to propel in any direction a miniature swimmer with flexible flagellum at a given minimal velocity. The proposed formulation is generic and can therefore be used for actuation devices with any number of coils in 2D or 3D situations. It was then applied to a case study and allowed to carry out new observations on the magnetic actuation of miniature swimmers. It showed that moving coils are of interest for the control of the swimmers, especially in biomedical applications.

Due to the use of coreless coils, magnetic couplings have been neglected. Nevertheless, the proposed criterion can be used as long as the couplings are taken into account while computing the magnetic field.

The proposed criterion is a first step towards new methods for the design and the control of miniature swimmers and gives several perspectives. First, this criterion is based on a minimal magnetic field constraint which can be formulated as the search of the Chebyshev ball in a zonotope. If such a problem can be formulated for other untethered swimmers or other robots, the proposed methodology could also be exploited. Moreover, these constraints are not strictly related to the use of magnetic fields. Indeed, any bounded constraint can be considered. Therefore, a first perspective is to extend this criterion to other devices. The second perspective is to study the design of magnetic navigation devices based on this criterion. Further discussions on the design of devices for the manipulation of the coils will be carried out and focus will be also given to the overall energy efficiency of such systems. Finally, swimmer control based on moving coil systems will be studied and experimental evaluations will be conducted. In particular, careful attention will be given to the different time constants obtained with both

actuation principles: the *a priori* slow reconfiguration of the coils and the fast current modulation.

ACKNOWLEDGMENT

This work is part of Multiflag project (ANR-16-CE33-0019) funded by the French National Research Agency (ANR) and supported by EIPHI Graduate School (Contract No. ANR-17-EURE-0002), by the COErCIVe région Bourgogne Franche-Comté project, by Labex CAMI (Contract No. ANR-11-LABX-0004) and the Grand Prix Scientifique 2018, Fondation Charles Defforey, Institut de France.

REFERENCES

[1] M. Sitti, "Miniature devices: Voyage of the microrobots," *Nature*, vol. 458, no. 7242, p. 1121, 2009.

[2] B. J. Nelson, I. K. Kaliakatsos, and J. J. Abbott, "Microrobots for Minimally Invasive Medicine," *Annual Review of Biomedical Engineering*, vol. 12, no. 1, pp. 55–85, 2010

[3] E. M. Purcell, "Life at low reynolds number," *American journal of physics*, vol. 45, no. 1, pp. 3–11, 1977.

[4] N. Chaillet and S. Regnier, *Microrobotics for Micromanipulation*. John Wiley & Sons, Mar. 2013.

[5] G. I. Taylor, "Analysis of the swimming of microscopic organisms," *Proceedings of the Royal Society of London. Series A. Mathematical and Physical Sciences*, vol. 209, no. 1099, pp. 447–461, Nov. 1951

[6] A. W. Mahoney and J. J. Abbott, "Five-degree-of-freedom manipulation of an untethered magnetic device in fluid using a single permanent magnet with application in stomach capsule endoscopy," *The International Journal of Robotics Research*, vol. 35, no. 1-3, pp. 129–147, 2016.

[7] M. P. Kummer, J. J. Abbott, B. E. Kratochvil, R. Borer, A. Sengul, and B. J. Nelson, "Octomag: An electromagnetic system for 5-dof wireless micromanipulation," *IEEE Transactions on Robotics*, vol. 26, no. 6, pp. 1006–1017, 2010.

[8] K. E. Peyer, L. Zhang, and B. J. Nelson, "Bio-inspired magnetic swimming microrobots for biomedical applications," *Nanoscale*, vol. 5, no. 4, pp. 1259–1272, 2013.

[9] Z. Zhang, X. Wang, J. Liu, C. Dai, and Y. Sun, "Robotic micromanipulation: Fundamentals and applications," *Annual Review of Control, Robotics, and Autonomous Systems*, vol. 2, pp. 181–203, 2019.

[10] D. Mahdy, S. Hesham, M. Mansour, A. Mohamed, I. Basla, N. Hamdi, I. S. Khalil, and S. Misra, "Characterization of helical propulsion inside in vitro and ex vivo models of a rabbit aorta," in *41st Annual International Conference of the IEEE Engineering in Medicine and Biology Society (EMBC)*, 2019, pp. 5283–8286.

[11] H. Lu, M. Zhang, Y. Yang, Q. Huang, T. Fukuda, Z. Wang, and Y. Shen, "A bioinspired multilegged soft millirobot that functions in both dry and wet conditions," *Nature communications*, vol. 9, no. 1, pp. 1–7, 2018.

[12] Y. Kim, H. Yuk, R. Zhao, S. A. Chester, and X. Zhao, "Printing ferromagnetic domains for untethered fast-transforming soft materials," *Nature*, vol. 558, no. 7709, pp. 274–279, 2018.

[13] J. J. Abbott, K. E. Peyer, M. C. Lagomarsino, L. Zhang, L. Dong, I. K. Kaliakatsos, and B. J. Nelson, "How should microrobots swim?" *The International Journal of Robotics Research*, vol. 28, no. 11-12, pp. 1434–1447, 2009.

[14] S. Martel, J.-B. Mathieu, O. Felfoul, A. Chanu, E. Aboussouan, S. Tamaz, P. Pouponneau, L. Yahia, G. Beaudoin, G. Soulez, *et al.*, "Automatic navigation of an untethered device in the artery of a living animal using a conventional clinical magnetic resonance imaging system," *Applied physics letters*, vol. 90, no. 11, p. 114105, 2007.

[15] B. E. Kratochvil, M. P. Kummer, S. Erni, R. Borer, D. R. Frutiger, S. Schürle, and B. J. Nelson, "Minimag: a hemispherical electromagnetic system for 5-dof wireless micromanipulation," in *Experimental Robotics*. Springer, 2014, pp. 317–329.

[16] E. Diller, J. Giltinan, G. Z. Lum, Z. Ye, and M. Sitti, "Six-degree-of-freedom magnetic actuation for wireless microrobotics," *The International Journal of Robotics Research*, vol. 35, no. 1-3, pp. 114–128, 2016.

[17] A. Pourkand and J. J. Abbott, "A critical analysis of eight-electromagnet manipulation systems: The role of electromagnet configuration on strength, isotropy, and access," *IEEE Robotics and Automation Letters*, vol. 3, no. 4, pp. 2957–2962, 2018.

[18] F. Ongaro, S. Pane, S. Scheggi, and S. Misra, "Design of an electromagnetic setup for independent three-dimensional control of pairs of identical and nonidentical microrobots," *IEEE Transactions on Robotics*, vol. 35, no. 1, pp. 174–183, 2018.

[19] S. E. Wright, A. W. Mahoney, K. M. Popek, and J. J. Abbott, "The spherical-actuator-magnet manipulator: A permanent-magnet robotic end-effector," *IEEE Transactions on Robotics*, vol. 33, no. 5, pp. 1013–1024, 2017.

[20] L. B. Kratchman, T. L. Bruns, J. J. Abbott, and R. J. Webster, "Guiding elastic rods with a robot-manipulated magnet for medical applications," *IEEE Transactions on Robotics*, vol. 33, no. 1, pp. 227–233, 2016.

[21] B. Véron, A. Hubert, J. Abadie, and N. Andreff, "Geometric analysis of the singularities of a magnetic manipulation system with several mobile coils," in *IEEE/RSJ International Conference on Intelligent Robots and Systems*, 2013, pp. 4996–5001.

[22] L. Yang, X. Du, E. Yu, D. Jin, and L. Zhang, "Deltamag: An electromagnetic manipulation system with parallel mobile coils," in *International Conference on Robotics and Automation*, 2019, pp. 9814–9820.

[23] J. Sikorski, C. M. Heunis, F. Franco, and S. Misra, "The armm system: An optimized mobile electromagnetic coil for non-linear actuation of flexible surgical instruments," *IEEE Transactions on Magnetics*, vol. 55, no. 9, pp. 1–9, 2019.

[24] T. Yoshikawa, "Manipulability of Robotic Mechanisms," *The International Journal of Robotics Research*, vol. 4, no. 2, pp. 3–9, June 1985

[25] J.-P. Merlet, "Jacobian, Manipulability, Condition Number and Accuracy of Parallel Robots," *ASME J. of Mechanical Design*, vol. 128, pp. 199–206, Jan. 2006.

[26] C. Gosselin and J. Angeles, "A Global Performance Index for the Kinematic Optimization of Robotic Manipulators," *J. Mech. Des*, vol. 113, no. 3, pp. 220–226, Sept. 1991.

[27] R. Chen, D. Folio, and A. Ferreira, "Performance metrics for a robotic actuation system using static and mobile electromagnets," in *International Conference on Robotics and Automation*, 2019, pp. 2474–2480.

[28] R. Dreyfus, J. Baudry, M. L. Roper, M. Fermigier, H. A. Stone, and J. Bibette, "Microscopic artificial swimmers," *Nature*, vol. 437, no. 7060, p. 862, 2005.

[29] C. P. Lowe, "Dynamics of filaments: modelling the dynamics of driven microfilaments," *Philosophical Transactions of the Royal Society of London. Series B: Biological Sciences*, vol. 358, no. 1437, pp. 1543–1550, 2003.

[30] M. Gouttefarde, J.-P. Merlet, and D. Daney, "Wrench-Feasible Workspace of Parallel Cable-Driven Mechanisms," in *Proceedings IEEE International Conference on Robotics and Automation*, Apr. 2007, pp. 1492–1497, iSSN: 1050-4729.

[31] S. Bouchard, C. Gosselin, and B. Moore, "On the Ability of a Cable-Driven Robot to Generate a Prescribed Set of Wrenches," *J. Mechanisms Robotics*, vol. 2, no. 1, Feb. 2010.

[32] P. McMullen, "On Zonotopes," *Transactions of the American Mathematical Society*, vol. 159, pp. 91–109, 1971.

[33] F. Christophersen, *Optimal Control of Constrained Piecewise Affine Systems*. Springer, Sept. 2007.

[34] M. Etiévant, A. Bolopion, S. Régnier, and N. Andreff, "An improved control-oriented modeling of the magnetic field," in *International Conference on Robotics and Automation*, May 2019, pp. 6178–6184.

[35] T. Xu, G. Hwang, N. Andreff, and S. Régnier, "Planar path following of 3-d steering scaled-up helical microswimmers," *IEEE Transactions on Robotics*, vol. 31, no. 1, pp. 117–127, 2015.